



**CHALMERS**  
UNIVERSITY OF TECHNOLOGY

## **Effect of Water on Local Structure and Dynamics in a Protic Ionic Liquid-Based Electrolyte**

Downloaded from: <https://research.chalmers.se>, 2026-04-15 07:44 UTC

Citation for the original published paper (version of record):

Lundin, F., Stettner, T., Falus, P. et al (2025). Effect of Water on Local Structure and Dynamics in a Protic Ionic Liquid-Based Electrolyte. *ChemSusChem*, 18(13).  
<http://dx.doi.org/10.1002/cssc.202402753>

N.B. When citing this work, cite the original published paper.

# Effect of Water on Local Structure and Dynamics in a Protic Ionic Liquid-Based Electrolyte

Filippa Lundin, Timo Stettner, Peter Falus, Andrea Balducci, and Aleksandar Matic\*

Ionic liquids (ILs) are promising candidates for electrolytes for next-generation energy storage and conversion systems. However, a high viscosity of the IL, hampering the ion transport, has led to strategies based on the dilution of the IL with a low-viscosity solvent. Herein, the influence of the addition of water to a protic IL to form a hybrid electrolyte suggested for supercapacitor applications is reported. The experiments directly test predictions from previous molecular dynamics simulations on this and other protic IL/water hybrid electrolytes. From small-angle X-ray scattering and infrared spectroscopy, it is shown that water is inserted in the ionic matrix

both as single molecules and in small aggregates. Water molecules hydrogen bonds to the available proton on the IL cation and effectively separates the ion pairs, resulting in an increase in the charge correlation distance. The change in the local structure is also reflected in the local dynamics probed by neutron spin-echo spectroscopy. A local diffusive-type process is revealed that correlates well with macroscopic ion transport, for example, the ionic conductivity. The results from neutron scattering also infer that the different local environments created by the addition of water have a relatively short lifetime.

## 1. Introduction

Ionic liquids (ILs) have been extensively investigated as electrolytes during the last decades.<sup>[1]</sup> Properties such as high thermal and electrochemical stability, low vapor pressure, and nonflammability are highly beneficial for application in next-generation energy storage and conversion systems with potential to improve both safety and performance.<sup>[2,3]</sup> A key property for electrolyte applications is fast ion transport and ILs in general will have lower ionic conductivity, compared to electrolytes based on organic solvents or aqueous electrolytes, as a result of a relatively high viscosity. The high viscosity can also cause issues with wetting of separator or infiltration of nanoporous electrodes. A common approach to mitigate these issues is to add a diluent. Mixtures of ILs and organic solvents have been proposed as hybrid

electrolytes, with faster ion transport being particularly important for high-power performance.<sup>[4–6]</sup> However, the addition of an organic solvent will compromise some of the beneficial properties of an IL electrolyte, for example, resulting in an increased flammability and safety concerns. In this respect, water is an attractive alternative as diluent, with further benefits of low cost and being nontoxic. Hybrid IL/water electrolytes have for instance recently been proposed for supercapacitors and Li-battery applications.<sup>[7,8]</sup>

The addition of water to an IL will already at low concentration change its physical properties. Even small amounts of water can lead to a drastic lowering of the viscosity and an increase of the conductivity. However, one can note that the addition of water can also be detrimental for some properties, such as a reduced electrochemical stability window.<sup>[8]</sup> The actual miscibility of water and IL strongly depends on the nature of constituent ions. A key property is the ability of forming hydrogen bonds between water and the cation and/or anion, to incorporate water in the ionic structure of the liquid. If there is no, or only weak, hydrogen bonding, formation of water clusters can be expected at relatively low water concentration, whereas water molecules can be well dispersed in the ionic network even close to equimolar concentrations in hydrogen bonding ILs.<sup>[9,10]</sup> In this context, protic ionic liquids (PILs) are of particular interest since they have an available proton, usually on the cation, enabling hydrogen bonding. Aprotic ILs are more common for electrolyte applications,<sup>[11]</sup> however, lately the interest in PILs has increased.<sup>[12–14]</sup>

A recent study reported on the influence of water on the physical and electrochemical properties of the PIL Pyr<sub>H4</sub>TFSI (1-butylpyrrolidinium bis(trifluoromethanesulfonyl)imide),<sup>[8]</sup> see **Scheme 1**. It was found that water improved capacity retention of a supercapacitor at high current densities, which was ascribed to improved transport properties. From molecular dynamics simulations, it was proposed that at lower water concentration, up to 2 wt% H<sub>2</sub>O that corresponds to a molar fraction of 0.3, water

F. Lundin, A. Matic  
Department of Physics  
Chalmers University of Technology  
412 96 Göteborg, Sweden  
E-mail: matic@chalmers.se

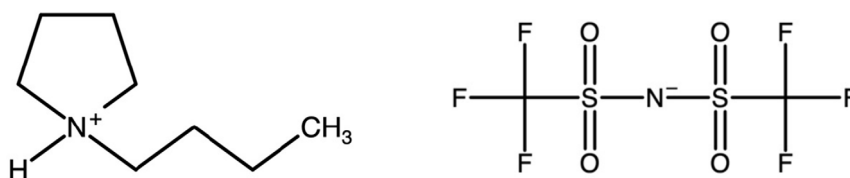
T. Stettner, A. Balducci  
Institute of Technical Chemistry and Environmental Chemistry  
Friedrich-Shiller-University Jena  
07743 Jena, Germany

T. Stettner, A. Balducci  
Center for Energy and Environmental Chemistry Jena  
07743 Jena, Germany

P. Falus  
Institut Laue-Langevin  
38042 Grenoble, France

Supporting information for this article is available on the WWW under <https://doi.org/10.1002/cssc.202402753>

© 2025 The Author(s). ChemSusChem published by Wiley-VCH GmbH. This is an open access article under the terms of the Creative Commons Attribution-NonCommercial License, which permits use, distribution and reproduction in any medium, provided the original work is properly cited and is not used for commercial purposes.



Scheme 1. Chemical structure of Pyr<sub>H4</sub> (left) and TFSI (right).

molecules are well dispersed and only small aggregates of few molecules could be identified. For higher concentrations, close to the solubility limit of 3.8 wt% H<sub>2</sub>O (corresponding to a molar fraction 0.5) larger aggregates (around 10 molecules) could be found.<sup>[15]</sup> In these larger aggregates, there are water molecules that are fully separated from the IL and that only interact with other water molecules in a more bulk-like fashion.<sup>[15]</sup> This is largely in agreement with atomistic simulation results on an imidazolium-based PIL with the same anion (TFSI).<sup>[10]</sup> This study suggests that water molecules coordinate both to the cation and the anion, interacting with the N and O atoms on the TFSI anion in addition to the proton on the cation, forming a bridge between the ions and inducing separation of ion pairs. This change in the nearest neighbor interactions, with weaker ion-ion interaction can potentially be linked to the improved ion transport. Thus, it is of interest to understand how the addition of water influences the nanostructure of the IL and the microscopic dynamics as the first step of macroscopic ion transport.

In this work, we investigate the influence of water on the local dynamics and nanostructure of the PIL Pyr<sub>H4</sub>TFSI to link the microscopic structure and dynamics to the macroscopic ion transport. A hallmark of ILs is the existence of ordering on length scales beyond the nearest neighbor correlations found in molecular liquids. This ordering is manifested as peaks in the static structure factor, typically in the range 0.1–1 Å<sup>-1</sup>, probed by for example, small-angle X-ray scattering (SAXS).<sup>[16–19]</sup> In ILs with shorter side chains on the cation, such as for Pyr<sub>H4</sub>TFSI which only has a butyl side chain, the nanostructure is related to charge ordering, that is, correlation between similar charges.<sup>[20,21]</sup> On these length scales ILs typically show quite complex dynamics with signatures of confined, or caged, dynamics preceding the more long-range diffusion.<sup>[22,23]</sup> Using SAXS and infrared spectroscopy (IR), we follow the influence of water on the local structure; and with neutron spin-echo spectroscopy (NSE), we probe microscopic dynamics on the typical time and length-scales found in ILs.

## 2. Results and Discussion

To investigate the influence of water on the nanostructure, and in particular, the charge ordering in the IL, SAXS measurement were performed. Figure 1 shows the SAXS patterns of the neat IL and the IL with addition of water at two different concentrations. In the neat IL, Pyr<sub>H4</sub>TFSI, the SAXS pattern shows two peaks, the molecular peak corresponding to nearest neighbor correlations around  $Q = 1.4 \text{ \AA}^{-1}$  and the charge ordering peak, from correlation of ions of similar charge (cation–cation and anion–anion), around  $Q = 0.85 \text{ \AA}^{-1}$ . There is no contribution in the SAXS pattern

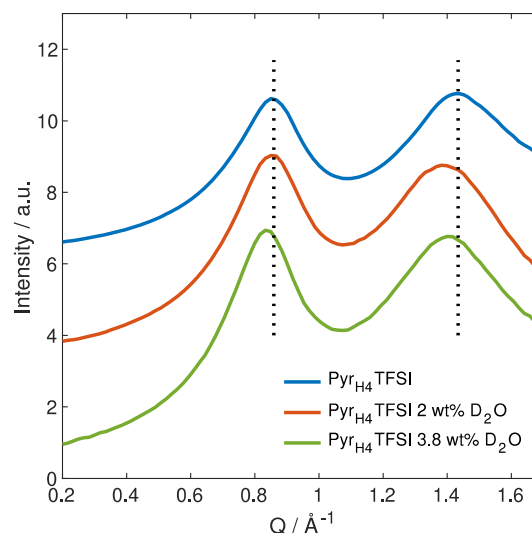


Figure 1. SAXS patterns for IL and D<sub>2</sub>O diluted IL at room temperature. Dotted lines mark the peak positions in the SAXS pattern of the neat IL. Data have been offset vertically for clarity.

from the formation of apolar domains, which is in agreement with the short alkyl side chain on the cation. The position of the charge ordering peak in the neat IL is shifted to slightly higher  $Q$  compared to what is found in the corresponding aprotic IL, Pyr<sub>14</sub>TFSI, where a methyl group is in the position of the proton on the pyrrolidinium ring, Figure S1, Supporting Information.<sup>[22,24]</sup> Thus, the charge correlation length in the neat IL is reduced by potential hydrogen bonding. The molecular peak is also shifted to slightly higher  $Q$ -values in the PIL compared to what is seen in the aprotic IL (1.4 vs 1.3 Å<sup>-1</sup> for the protic and aprotic ILs, respectively), indicating a closer packing of nearest neighbors which can be a result of hydrogen bond interaction between cation and anion.

The SAXS patterns of the IL/water mixtures show very similar features to the neat IL. This is in agreement with previous studies on an aprotic IL where no larger structural changes were found as up to 50 mol% of water was added.<sup>[25]</sup> However, there is a progressive shift in the peak positions of both the molecular and the charge ordering peak toward smaller  $Q$ -values with the amount of water added. The shift of the molecular peak to smaller  $Q$ -values indicates an increased distance between nearest neighbors and correlates well with the decrease in the density with the addition of water reported previously.<sup>[8]</sup> A minute shift to higher  $Q$  can be noted for the IL with 3.8 wt% water compared to 2 wt% water. This is most likely connected to a small contribution of water to the SAXS pattern at high  $Q$ . Similarly, the shift to lower  $Q$ -values of the charge ordering peak implies an increase in the

distance between similar charges. Yaghini et al, showed that the preferential interaction site of water in the PIL,  $C_2HmTFSI$ , is the  $-NH$  group of the cation<sup>[26]</sup> and a similar situation can be expected for  $Pyr_{H4}TFSI$ . The cation then effectively becomes larger with the water bonded to it, and therefore, the distances between the charges are expected to be larger. The water molecules can also bridge between cation and anion, as suggested by computer simulations,<sup>[10,15]</sup> inducing further charge separation, increasing the charge correlation distance. One can note that no new features related to the development of water domains can be seen in the SAXS patterns. Previous molecular dynamics simulations on this system predicted the existence of aggregates with an average size of up to 10–15 molecules for the highest water concentration (3.8 wt%  $H_2O$ ),<sup>[8]</sup> which would correspond to a domain size of around 8–10 Å. In the SAXS pattern, this would show up on the low- $Q$  side of the charge ordering correlation peak. However, no sign of an additional peak, or a broadening of the charge ordering peak, can be discerned. The existence of water aggregates can, however, not be ruled out based on this data as a distribution in domain sizes would result in a rather diffuse contribution overlapping with the charge ordering peak.

To further investigate the local structure and coordination in the IL/water mixtures, IR spectroscopy was used and **Figure 2** shows spectra in the region 2600–3800  $cm^{-1}$ . The most notable influence on the spectra by the addition of water is the broad band appearing at 3580  $cm^{-1}$  which increases with increased water content. This band is related to the OH-stretch vibration of water molecules. Compared to the spectrum of bulk water this contribution is centered at higher wavenumbers. In bulk water, the very broad OH-stretch band is a result of the strong hydrogen bonding network which shifts the vibration to lower wavenumbers. This shows that in the IL/water mixtures the water molecules are rather well dispersed, and we do not have a bulk-like water phase. One should note that a small signature of the OH-stretch band can also be seen in the neat IL, related to that the measurements were performed at ambient conditions where water from the atmosphere can contribute to the signal.

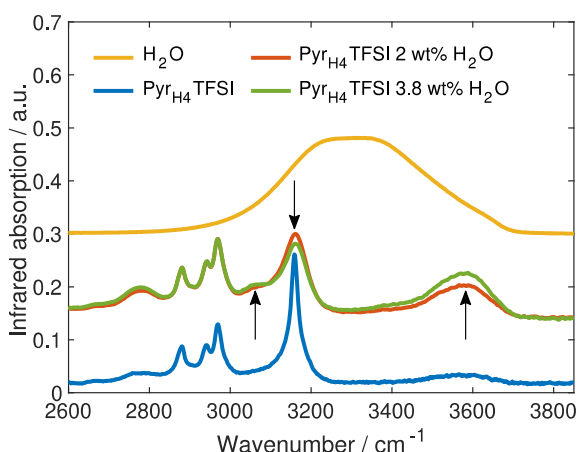


**Figure 2.** IR spectra of neat IL and IL/water mixtures. Arrows indicate trends with increased water concentration. Spectrum of  $H_2O$  is added for comparison and the spectra of neat IL and water are vertically offset for clarity.

The interaction between water and the IL cation can be observed from the behavior of the band at 3160  $cm^{-1}$  and appearance of a new band at 3060  $cm^{-1}$  with the addition of water.

The band at 3160  $cm^{-1}$  originates from the N–H stretch vibration on the pyrrolidinium ring of the cation. One could have expected an even higher intensity of the 3060  $cm^{-1}$  band if water was fully dispersed in the ionic structure, that is, each cation hydrogen bonds with one water molecule. This supports the findings of MD-simulations on water mixtures with  $Pyr_{H4}TFSI$  which suggest the presence of small clusters of water, from a few water molecules bridging between anion and cation of the IL to aggregates of around 10 molecules dispersed in the ionic matrix.<sup>[15]</sup> One can note that the N–H stretch band at 3160  $cm^{-1}$  in fact broadens with the addition of water, suggesting a distribution of environments with more or less hydrogen-bonded cations. Cations interacting with water molecules in small aggregates will experience weaker hydrogen bonding and with only a small shift of the N–H band as a result.

The changes in the local structure and interactions can be expected to influence the ion transport. Indeed, previous studies of this IL have shown an increase in the ionic conductivity with the addition of water.<sup>[8]</sup> From molecular dynamics simulations, it is suggested that this is also reflected in faster local ion dynamics.<sup>[15]</sup> Here, we investigate the microscopic dynamics on the molecular scale using neutron spin-echo spectroscopy (NSE) which covers pico- to nanosecond time scales and the length scales corresponding to the nanostructure of the IL. For the IL incoherent scattering from the cation dominates the signal in the experiment, due to the strong contribution of the H-atoms on  $Pyr_{H4}$ . In the IL/water mixtures, deuterated water has been used to decrease the contribution from water to the scattering, hence also here the signal is dominated by cation dynamics. With predominantly incoherent scattering this experiment probes the self-correlations in the system, such as self-diffusion.<sup>[27]</sup> Information about the scattering cross-sections of all samples is found in Table S1 and S2, Supporting Information. With the addition of  $D_2O$  deuterium/proton exchange between  $Pyr_{H4}$  and  $D_2O$  can in principle occur for the acidic proton on the nitrogen of the cation whereas the probability of exchange with protons on the ring and the butyl chain is low. In addition, even at the highest water concentration in the IL, the ratio between protons and deuterium is 9:1 (3.8 wt% of water corresponds to 0.5 in molar fraction). Thus, the influence on the scattering cross-sections of a potential exchange would be rather small and the cation still accounts for the vast majority of the incoherent scattering.

**Figure 3a** shows the intermediate scattering functions of the IL with varying water content. The water-containing samples show slightly faster dynamics compared to the neat IL, which agrees well with what is seen for the macroscopic transport, that is, the conductivity.<sup>[8]</sup> The temperature dependence of the intermediate scattering function of  $Pyr_{H4}TFSI$  is shown in **Figure 3b**, revealing a strong temperature dependence with faster dynamics at higher temperatures. **Figure 3c** shows the momentum transfer,  $Q$ , dependence of the intermediate scattering function, which provides information about the nature of the motion. A faster relaxation with increasing  $Q$ , as seen here, is a typical sign of a diffusive motion.<sup>[27]</sup>

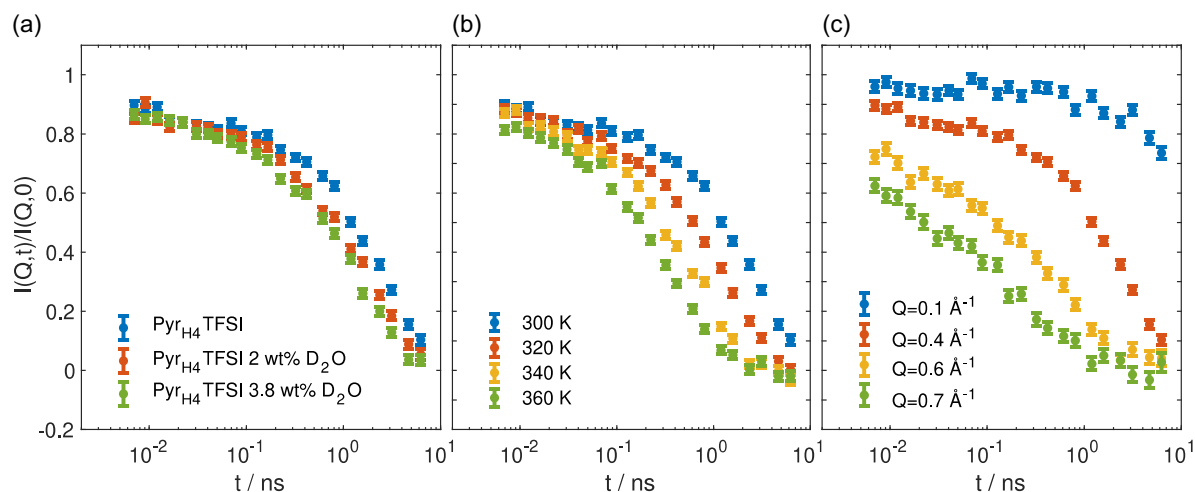


**Figure 3.** Intermediate scattering functions of Pyr<sub>H4</sub>TFSI and Pyr<sub>H4</sub>TFSI /D<sub>2</sub>O mixtures a) for different D<sub>2</sub>O concentration at 300 K and  $Q = 0.35 \text{ \AA}^{-1}$ , b) for different temperatures at  $Q = 0.35 \text{ \AA}^{-1}$ , and c) different momentum transfer at 300 K for Pyr<sub>H4</sub>TFSI.

To extract the relaxation times, as a function of temperature and momentum transfer, the intermediate scattering functions were fitted to Equation (1) and (2), depending on the momentum transfer, see further below.

$$\frac{I(Q,t)}{I(Q,0)} = A \cdot e^{-\left(\frac{t}{\tau_1}\right)^\beta} + (1-A) \cdot e^{-\left(\frac{t}{\tau_2}\right)} \quad Q < 0.8 \text{ \AA}^{-1} \quad (1)$$

$$\frac{I(Q,t)}{I(Q,0)} = A \cdot e^{-\left(\frac{t}{\tau_1}\right)^\beta} + (1-A+B) \cdot e^{-\left(\frac{t}{\tau_2}\right)} - B \cdot e^{-\left(\frac{t}{\tau_3}\right)} \quad Q = 0.8 \text{ \AA}^{-1} \quad (2)$$

The first term is a stretched exponential function, with stretching parameter  $\beta$ , and the second term is a single exponential function. The stretched exponential function has successfully been used for ILs to capture slower diffusive type relaxations,<sup>[28]</sup> whereas the single exponential relaxation captures local dynamics at short time scales.<sup>[29,30]</sup> At the highest momentum transfer,  $Q = 0.8 \text{ \AA}^{-1}$ , the scattering function goes slightly negative, Figure S3, Supporting Information, and a different fitting function is needed. This is related to a coherent contribution, that appears as negative as a result of the normalization of the neutron spin-echo signal by the neutron polarization in the case of a predominantly incoherent scattering. The effect is rather weak (less than 10% of scattering is coherent) and it thus appears only when the coherent scattering is stronger, that is, when the static structure factor increases toward the charge correlation peak, and the incoherent contribution is low (end of relaxation function). To properly fit the scattering function in this case a third negative contribution that takes the coherent contribution into account is added according to Equation (2). Figure S2 and S3, Supporting Information, show representative fits of the intermediate scattering functions.

Results from the fits of the scattering functions are shown in **Figure 4**. The fast relaxation,  $\tau_2$ , has no or very weak temperature, concentration, and momentum transfer dependence. The momentum transfer independence is a signature of a local process and has been assigned to for instance libration of the ring

on the cation or relaxation of the butyl side chain for the aprotic analogue IL Pyr<sub>14</sub>TFSI.<sup>[22]</sup> In contrast, the slower relaxation,  $\tau_1$ , shows a concentration dependence, and strong momentum transfer and temperature dependencies. The relaxation function is only slightly stretched with a stretching parameter in the range 0.7–0.85, see Figure S4, Supporting Information, reflecting a rather small distribution of relaxation times and a not very pronounced dynamical heterogeneity. There is no evident temperature or concentration dependence of the stretching parameter ( $\beta$ ) which can be explained by the fact that the experiments are performed above the melting point, that is, not in the supercooled liquid where one expects an increased dynamic heterogeneity with temperature.<sup>[32]</sup> The absence of a concentration dependence is potentially more surprising. IR spectroscopy suggests that there are in fact different cation environments with the addition of water, cations experiencing different degrees of hydrogen bonding. The fact that this does not seem to lead to an increase in the dynamical heterogeneity suggests that the lifetime of these environments is shorter than the time scale of the diffusive process observed here, that is, that there is a rapid exchange in the coordinating shell around the cation. Thus, in the NSE experiment, we probe the average dynamics over these different environments. The stretching parameter also shows a momentum transfer dependence, with a slight decrease with  $Q$ . This is in agreement with previous reports and relates to an increased heterogeneity of the dynamics as shorter length scales are probed at higher momentum transfers.<sup>[31]</sup>

In Figure 4, the mean relaxation time,  $\langle \tau_1 \rangle$ , of the slow relaxation is reported. It takes the stretching parameter,  $\beta$ , into account according to

$$\langle \tau_1 \rangle = \Gamma\left(\frac{1}{\beta}\right) \cdot \frac{1}{\beta} \cdot \tau_1 \quad (3)$$

where  $\Gamma$  is the gamma function. The momentum transfer dependence of the mean relaxation time  $\langle \tau_1 \rangle$  is shown in Figure S5, Supporting Information, revealing a decrease in the relaxation

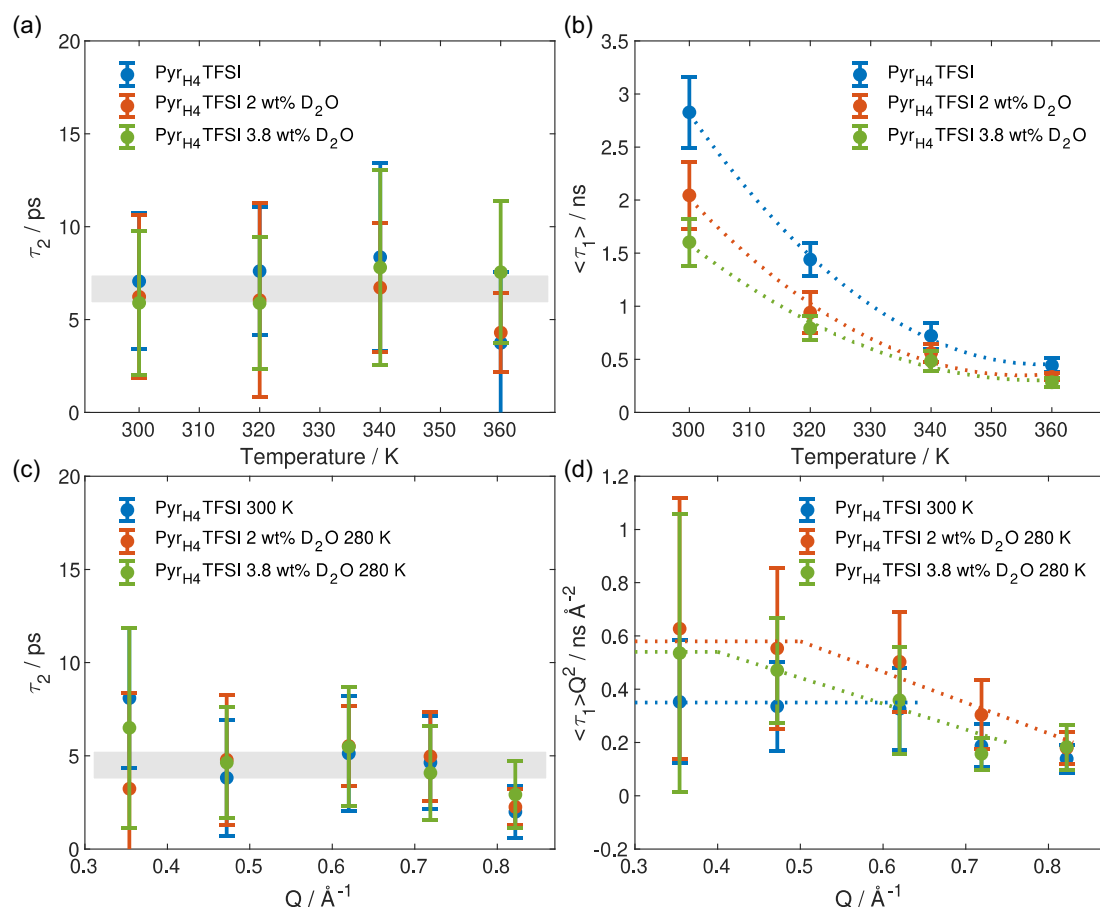


**Figure 4.** Results from fits of the intermediate scattering functions of  $\text{Pyr}_{\text{H4}}\text{TFSI}$  and  $\text{Pyr}_{\text{H4}}\text{TFSI}$  with  $\text{D}_2\text{O}$ . Temperature dependence of a) relaxation time of the fast relaxation,  $\tau_2$  and b) average relaxation time of the slow relaxation,  $\langle\tau_1\rangle$ , at  $Q = 0.35 \text{ \AA}^{-1}$ . c) Momentum transfer dependence on the relaxation time of the fast relaxation,  $\tau_2$ . d) Momentum transfer dependence of average relaxation time multiplied with  $Q^2$ ,  $\langle\tau_1\rangle Q^2$ . Average relaxation times are calculated using Equation (3). Gray bands and dotted lines are guides to the eye.

time with increasing  $Q$ . For a Fickian diffusion process,  $\langle\tau_1\rangle \propto Q^{-2}$  is expected<sup>[27]</sup> and in Figure 4d  $\langle\tau_1\rangle Q^2$  is plotted versus  $Q$ . One should note that data for the momentum transfer dependence is compared at similar relaxation times, that is, different temperatures, between the neat and the hydrated IL, to have the full relaxation process in the dynamic window of the instrument for all momentum transfers. For the neat IL, a strong momentum transfer dependence of the mean relaxation time is observed (Figure S5, Supporting Information). It follows the prediction for a Fickian diffusion process,  $\langle\tau_1\rangle Q^2 = \text{constant}$ , at low momentum transfers, up to  $Q = 0.6 \text{ \AA}^{-1}$ , Figure 4d. The same data are shown in the more traditional representation as  $\langle\tau_1\rangle^{-1}$  versus  $Q^2$  in Figure S6, Supporting Information. A similar behavior has previously been reported by Kofu et al. for a neat IL and was proposed to be related to a transition from Fickian diffusion to Gaussian dynamics.<sup>[31]</sup> With the addition of water, the momentum transfer dependence of the average relaxation time is weaker, and we no longer observe the regime of simple diffusion, reflecting an increase in the heterogeneity of the local environment. The crossover is just at the edge of our momentum transfer window and seems to occur at progressively lower momentum transfers with increasing water concentration.

The relaxation time as a function of temperature and water concentration is shown in Figure 4b. As expected for a diffusive type process the relaxation time decreases with temperature, congruent with the behavior of macroscopic transport properties, with an increase in conductivity and decrease in viscosity.<sup>[8]</sup> The addition of water results in faster dynamics both on the macro- and microscopic length scales. To quantitatively investigate the influence of water on the dynamics, Figure 5 reports the relative change of the mean relaxation time and the conductivity for the water-containing samples with respect to the neat IL. Overall, the micro- and macroscopic dynamics follow each other as a function of temperature and water concentration. The addition of water seemingly has a stronger effect on the microscopic dynamics, with a relative increase of  $\approx 1.7$  at the highest water concentration for the relaxation time compared to  $\approx 1.5$  for the conductivity. In this comparison, one needs to take into account that the neutron scattering experiment probes only the diffusive dynamics of the IL cation, whereas the conductivity also has a contribution from the diffusive motion of the anion. In addition, when water is added the number of charge carriers is decreased whereas the local dynamics of the ions are faster. Thus, the overall increase in the conductivity can be expected to be lower.

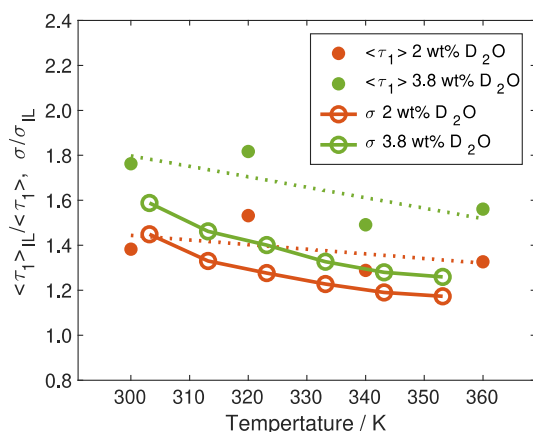


**Figure 5.** Relative change in mean relaxation time at  $Q = 0.35 \text{ \AA}^{-1}$  of the Pyr<sub>H4</sub> cation and conductivities for the water-containing electrolytes. The mean relaxation time and conductivities have been scaled with values obtained for the neat IL Pyr<sub>H4</sub>TFSI.

### 3. Conclusion

The influence on the local structure, interactions, and microscopic dynamics by the addition of water to a PIL electrolyte has been experimentally investigated. Previous simulation results have suggested the presence of both dispersed water molecules in the ionic matrix as well as the existence of smaller aggregates of water. From SAXS experiments, we observe an increase in the charge correlation distance supporting the suggestion that water molecules are dispersed in the ionic matrix separating ion pairs. The coordination of water to the IL cation is supported by results from IR spectroscopy. It shows upon hydrogen bonding between water molecules and the IL cations and indicates the existence of both fully dispersed water molecules (interacting only with one cation) and water present in pairs or in smaller aggregates. We do not see evidence of larger aggregates as these would contribute to the SAXS signal. Using NSE, we also directly probe the dynamics of the IL cation on the length scales of the local structure. For the neat IL, we observe Fickian-like diffusion at low momentum transfers, with a transition to more heterogeneous dynamics toward the distances corresponding to charge ordering. With the addition of water, this crossover shifts to lower momentum transfers, reflecting heterogeneous dynamics on longer length scales. The results from neutron scattering also infer that the different local environments created by the addition of water have a relatively short lifetime, since the shape of the relaxation function does not change as water is added. Similarly, a local fast relaxation of the IL cation is observed which does not change with the addition of water. We also show that the influence of water on the local dynamics in the IL is directly reflected in the behavior of the macroscopic ion transport.

## 4. Experimental Section

### Materials

1-butylpyrrolidinium bis(trifluoromethanesulfonyl)imide (Pyr<sub>H4</sub>TFSI) was synthesized following the procedure described previously.<sup>[32]</sup>

The IL, Pyr<sub>H4</sub>TFSI, was mixed with 2.0 and 3.8 wt% D<sub>2</sub>O for the NSE and SAXS experiment and with H<sub>2</sub>O for the IR experiment. All samples were prepared and kept in closed vials in inert atmosphere to keep the water concentration constant.

### IR Spectroscopy

A single reflection diamond crystal attenuated total reflectance (ATR) unit, Golden Gate from Specac, and a Fourier transform infrared spectroscopy (FTIR) spectrometer model IFS 66 v S<sup>-1</sup> from Bruker were used to collect ATR-FTIR spectra. The measurements were performed at room temperature with a resolution of 2 cm<sup>-1</sup> for the neat IL and 4 cm<sup>-1</sup> for the water-containing samples.

### Small Angle X-ray Scattering (SAXS)

SAXS was performed on a Mat:Nordic instrument from SAXSLAB with a Rigaku 003+ high brilliance microfocus Cu-radiation source and a Pilatus 300 K detector. The samples were filled in 1.5 mm diameter glass capillaries (sealed with wax in inert atmosphere) and measured at room temperature for 30 min.

### Neutron Spin-Echo Spectroscopy (NSE)

NSE was performed on the WASP spectrometer, ILL, France.<sup>[33]</sup> Two wavelengths, 7 and 5 Å were used, resulting in a time window of 3 ps to 6 ns and a momentum transfer range of  $Q = 0.1\text{--}0.8 \text{ \AA}^{-1}$  was used. Data were collected in the temperature range 280–360 K for the water-containing samples and 300–360 K for the neat IL. Annular aluminum cans with thickness of 0.2 mm were used. Measurements of empty cell and cadmium were used for background subtraction and a TiZr sample was used for resolution.

Data were reduced using an ILL-developed software based on the commercial software package Igor Pro 8<sup>[34]</sup> and fitted using MATLAB. Neutron cross-sections for the different samples are found in Table S1 and S2, Supporting Information.

### Acknowledgements

This work was financially supported by the Swedish Foundation for Strategic Research (SSF) within the Swedish National Graduate School in Neutron Scattering (SwedNess) grant no. G5n15-0008 and Deutsche Forschungsgemeinschaft (DFG) within the project BA4956/10-1. The authors also thank Ezio Zanghellini for support with FTIR measurements.

### Conflict of Interest

The authors declare no conflict of interest.

### Data Availability Statement

The data that support the findings of this study are available from the corresponding author upon reasonable request.

**Keywords:** electrolytes · ionic liquids · materials science · neutron spin-echo spectroscopy

- [1] Z. Lei, B. Chen, Y. M. Koo, D. R. Macfarlane, *Chem. Rev.* **2017**, *117*, 6633.
- [2] A. Matic, B. Scrosati, *MRS Bull.* **2013**, *38*, 533.
- [3] E. Jónsson, *Energy Storage Mater.* **2020**, *25*, 827.
- [4] L. Aguilera, J. Scheers, A. Matic, *Phys. Chem. Chem. Phys.* **2016**, *18*, 25458.
- [5] C.-J. Wu, P. C. Rath, J. Patra, D. Bresser, S. Passerini, B. Umesh, Q.-F. Dong, T.-C. Lee, J.-K. Chang, *ACS Appl. Mater. Interfaces* **2019**, *11*, 42049.
- [6] S. Pan, M. Yao, J. Zhang, B. Li, C. Xing, X. Song, P. Su, H. Zhang, *Front. Chem.* **2020**, *8*, 261.
- [7] M. Becker, D. Rentsch, D. Reber, A. Aribia, C. Battaglia, R.-S. Kühnel, *Angew. Chem. Int. Ed.* **2021**, *60*, 14100.
- [8] T. Stettner, S. Gehrke, P. Ray, B. Kirchner, A. Balducci, *ChemSusChem* **2019**, *12*, 3827.
- [9] J. Gao, N. J. Wagner, *Langmuir* **2016**, *32*, 5078.
- [10] H. E. Bailey, Y.-L. Wang, M. D. Fayer, *J. Phys. Chem. B* **2017**, *121*, 8564.
- [11] A. Balducci, *Top. Curr. Chem.* **2017**, *375*, 20.
- [12] T. L. Greaves, C. J. Drummond, *Chem. Rev.* **2015**, *115*, 11379.
- [13] B. Gorska, J. Pernak, F. Béguin, *Electrochim. Acta* **2017**, *246*, 971.
- [14] A. Djire, J. Y. Ishimwe, S. Choi, L. T. Thompson, *Electrochem. Commun.* **2017**, *77*, 19.
- [15] S. Gehrke, P. Ray, T. Stettner, A. Balducci, B. Kirchner, *ChemSusChem* **2021**, *14*, 3315.
- [16] O. Russina, A. Triolo, L. Gontrani, R. Caminiti, *J. Phys. Chem. Lett.* **2012**, *3*, 27.
- [17] A. Triolo, O. Russina, B. Fazio, G. B. Appetecchi, M. Carewska, S. Passerini, *J. Chem. Phys.* **2009**, *130*, 164521.
- [18] A. Triolo, O. Russina, H.-J. Bleif, E. Di Cola, *J. Phys. Chem. B* **2007**, *111*, 4641.
- [19] O. Russina, A. Triolo, *Faraday Discuss.* **2011**, *154*, 97.
- [20] H. K. Kashyap, J. J. Hettige, H. V. R. Annapureddy, C. J. Margulis, *Chem. Commun.* **2012**, *48*, 5103.
- [21] J. J. Hettige, H. K. Kashyap, H. V. R. Annapureddy, C. J. Margulis, *J. Phys. Chem. Lett.* **2013**, *4*, 105.
- [22] F. Lundin, H. W. Hansen, K. Adrjanowicz, B. Frick, D. Rauber, R. Hempelmann, O. Shebanova, K. Niss, A. Matic, *J. Phys. Chem. B* **2021**, *125*, 2719.
- [23] M. Sha, X. Ma, N. Li, F. Luo, G. Zhu, M. D. Fayer, *J. Chem. Phys.* **2019**, *151*, 154502.
- [24] L. Aguilera, J. Völkner, A. Labrador, A. Matic, *Phys. Chem. Chem. Phys.* **2015**, *17*, 27082.
- [25] O. Borodin, D. L. Price, B. Aoun, M. A. González, J. B. Hooper, M. Kofu, S. Kohara, O. Yamamuro, M.-L. Saboungi, *Phys. Chem. Chem. Phys.* **2016**, *18*, 23474.
- [26] N. Yaghini, L. Nordstierna, A. Martinelli, *Phys. Chem. Chem. Phys.* **2014**, *16*, 9266.
- [27] M. T. F. Telling, *A Practical Guide to Quasi-Elastic Neutron Scattering*, Royal Society of Chemistry, Croydon, UK **2020**.
- [28] M. Kofu, M. Nagao, T. Ueki, Y. Kitazawa, Y. Nakamura, S. Sawamura, M. Watanabe, O. Yamamuro, *J. Phys. Chem. B* **2013**, *117*, 2773.
- [29] M. Kofu, M. Tyagi, Y. Inamura, K. Miyazaki, O. Yamamuro, *J. Chem. Phys.* **2015**, *143*, 234502.
- [30] P. Luo, Y. Zhai, P. Falus, V. García Sakai, M. Hartl, M. Kofu, K. Nakajima, A. Faraone, Y. Z. *Nat. Commun.* **2022**, *13*, 2092.
- [31] M. Kofu, A. Faraone, M. Tyagi, M. Nagao, O. Yamamuro, *Phys. Rev. E* **2018**, *98*, 42601.
- [32] L. Timperman, P. Skowron, A. Boisset, H. Galiano, D. Lemordant, E. Frackowiak, F. Béguin, M. Anouti, *Phys. Chem. Chem. Phys.* **2012**, *14*, 8199.
- [33] F. Lundin, A. Balducci, P. Falus, A. Matic, T. Stettner, *Influence of Water on the Dynamics of a Protic Ionic Liquid*, Institute Laue-Langevin (ILL) **2021**.
- [34] P. Fouquet, G. Ehlers, B. Farago, C. Pappas, F. Mezei, *J. Neutron Res.* **2007**, *15*, 39.

---

Manuscript received: December 28, 2024  
Revised manuscript received: April 2, 2025  
Version of record online: April 8, 2025